

LOCALIZED MHD ACTIVITY NEAR TRANSPORT BARRIERS IN JT-60U AND TFTR

J. Manickam, T. Fujita¹, N. Gorelenkov, A. Isayama¹, Y. Kamada¹, M. Okabayashi, M. Bell, R. Bell, R. Budny, E. Fredrickson, S. Ishida¹, Y. Ishii¹, F. Levinton², T. Ozeki¹, H. Shirai¹, S. Takeji¹ and M. Zarnstorff

Princeton Plasma Physics Laboratory, Princeton, NJ USA

¹ *Japan Atomic Energy Research Institute, Naka, Japan*

² *Fusion Physics and Technology, Torrance, CA USA*

Abstract

Localized MHD activity observed in JT-60U and TFTR near transport barriers with their associated large pressure gradients is investigated. Stability analysis of equilibria modeling the experiments supports an identification of this MHD as being due to an ideal MHD $n = 1$ instability. The appearance of the instability depends on the local pressure gradient, local shear in the q profile and the proximity of rational surfaces where $q \sim m/n$ and m and n are the poloidal and toroidal mode numbers respectively. The mode width is shown to depend on the local value of q , and is larger when q is smaller. In addition the role of the edge current density in coupling the internal mode to the plasma edge and of the energetic particles which can drive fishbone like modes is investigated.

1 Experimental Observations

The reversed shear configuration in association with improved confinement through internal transport barriers, (ITB), is considered an attractive candidate for tokamak fusion reactors. Previous studies on JT-60U[1,2] and TFTR[3] have shown that the highest achievable β in this configuration is generally determined by low- n ideal MHD instabilities which are global in nature. At lower values of β a variety of other MHD events may also occur. These include double tearing modes during the early phase of the discharge, neo-classical tearing modes during the high-power heating phase as well as off-axis sawtooth-like crashes. Many of these observations have been described in earlier works[4,5,6,7]. In addition, careful observations in both JT-60U and TFTR reveal localized MHD activity often occurring in brief bursts in the vicinity of the transport barrier, which may affect the discharge by inducing a momentary loss in local confinement, or a minor “beta collapse”, and may also affect the maximum stored energy achieved in the discharge[1]. In this report we concentrate on these burst-like modes and refer to them as BLMs, as they are *Barrier Localized Modes*.

Figure 1 shows the complete time history of one of the highest achieving discharges in JT-60U. The points to note are that the BLMs occur well below the maximum stored energy, and are localized in the radial extent. Note that the T_e trace at $r/a = 0.11$ is unaffected while the traces corresponding to $r/a = 0.29$ and 0.49 show sharp jumps. The jumps in T_e are coincidental with MHD bursts observed on the Mirnov diagnostic. The mode is determined to have a toroidal mode number of unity. The bursts are often seen to coincide with q_{\min} having an integer value, in this case $q_{\min} \sim 4$. Although in this example there is no β -collapse, some discharges on JT-60U display a collapse i.e. a momentary loss of a significant amount of stored energy. These events are localized to the vicinity of the transport barrier, in this case approximately at $r/a = 0.6$, and the $T_e(r)$ profile is locally flattened within a time period of less than one millisecond. Similar observations have been made on TFTR.

Figure 2 shows an expanded view of BLMs in TFTR and JT-60U. The first three panels of this figure show time traces of the electron temperature at three selected radii, the Mirnov loop measurement and its power spectrum. The last panel on each side shows a time-expanded view

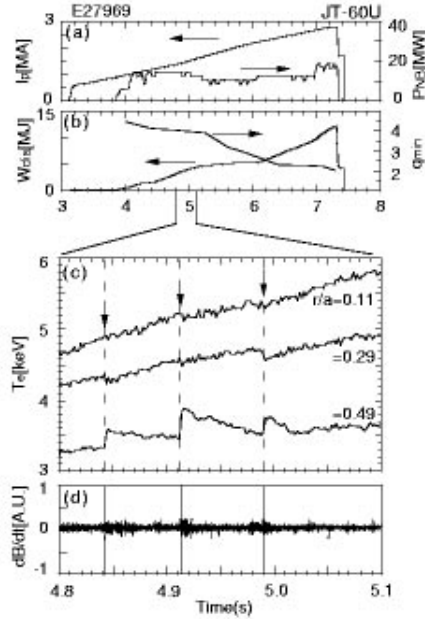


Figure 1: Time evolution of the (a) plasma current, I_p , neutral beam injection power P_{NB} , (b) stored energy, W_{dia} , and q_{min} on JT-60U for the length of the discharge. Panels (c) and (d) show an expanded view of a shorter time segment, where (c) has the evolution of T_e at three radii, and (d) shows the data from a Mirnov loop. Note the spatial localization and inversion in the T_e traces. The Mirnov activity coincides with the T_e bursts.

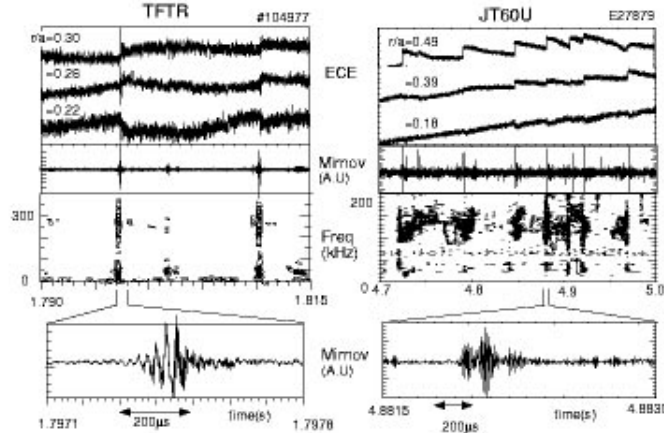


Figure 2: Traces of T_e and the Mirnov activity on TFTR and JT-60U showing the similar burst-like features of BLMs in both devices. Note the spatial localization and inversion in the T_e traces. The Mirnov activity coincides with the T_e bursts and the mode is seen to grow on a time scale shorter than $100\mu s$.

of the Mirnov data for a single burst. The data shows that in a very brief period, less than a millisecond the temperature drops on an inner surface and rises on the outside. The temperature at even larger radii, (not shown), is unaffected. The bursts are temporally correlated on the Mirnov and T_e traces and last for less than a millisecond.

While many features of BLMs are similar in the two devices there are some differences.

Compared to JT-60U BLMs were less frequently observed in TFTR. Further, the BLMs on TFTR sometimes had a very clear fishbone like structure and in some cases they were associated with the observation of intense radial electric fields as seen in Fig. 3. This feature will be discussed in Sec. 2.

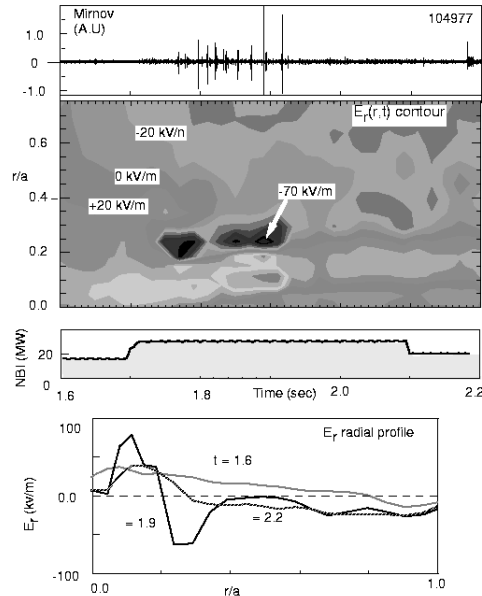


Figure 3: The BLM activity in TFTR sometimes coincides with intense negative radial electric fields. The top trace shows the Mirnov signal, the middle panel shows contours of the radial electric field which changes with time. The radial profile of E_r at times corresponding to the BLMs is shown in the lowest panel. Note that while the field shown here has a maximum negative value of 60kV/m ; in some bursts, field strengths in excess of 100kV/m have been observed.

In both experiments these modes are associated with low- n , typically $n = 1$, MHD activity, and the poloidal mode number according to the Mirnov data is $m \sim q_{\text{edge}}$. In both experiments precursors and post-cursors are sometimes observed, although some shots have no oscillatory precursor. This is analogous to the observation with sawteeth, with the difference that the relaxation of T_e is localized and does not extend to the core. In both experiments when an oscillatory precursor is observed it has a growth-time in the range $50\text{-}100\mu\text{s}$ suggesting that it may be an ideal MHD instability.

It is interesting to note that during the high- β_p mode of operation in JT-60U, which is characterized by a strong ITB for ion transport in the region of weak *positive* shear, similar BLMs were also observed[7], suggesting that it is the low shear that matters, regardless of the sign.

2 Analysis

The experimental observations clearly indicate that the *local* value of the pressure gradient, rather than the global β , is a critical parameter, coupled with the low shear and the proximity of low- n rational surfaces. We now present detailed analysis for specific discharges. We discuss the ideal MHD stability of two shots JT-60U:27969 and TFTR:96051. The theoretical analysis starts with equilibria which characterize these discharges. Figure 4 shows the profiles at the

time when BLMs are observed in the experiment. The q -profile is determined from the MSE observations and the pressure profile is obtained from self-consistent transport calculations using TOPICS[8] for JT-60U and TRANSP[9] for TFTR data. Ideal MHD stability analysis using the PEST[10] code shows that both the equilibria are unstable to an $n = 1$ mode with growth-times ranging from 50 to 300 μ s. The boundary conditions for this and subsequent analyses correspond to having a wall at infinity. The growth-times should be treated with caution for two reasons. First the modeling of the experiment is subject to an inherent uncertainty arising from the data interpretation. Second small changes in profile parameters near marginal stability will cause large relative changes in the growth-times. The important point is that the growth-times are in the ideal MHD range and correspond approximately to the experimental observations. The radial structure of the instability is also shown in Fig. 4. The key aspects which agree with the experimental observation are that the mode peaks at a radius which corresponds to the maximum pressure gradient, which lies just outside the transport barrier. This location also coincides with the low shear region. The poloidal mode number varies depending on the local- q value so that $m \sim q_{\text{local}}$. The availability of ECE data on a fast time scale, 500 kHz, on TFTR allows us to reconstruct the displacement vector from the T_e fluctuations. The results are also shown in Fig. 4, and compare very favorably with the theoretical mode structure.

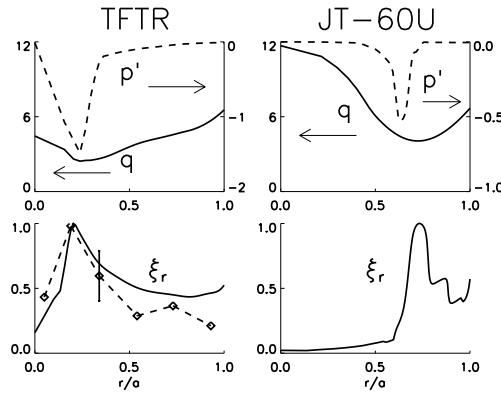


Figure 4: Plasma p and q profiles at the time of a BLM in TFTR and JT-60U and the radial component of the displacement vector for an $n = 1$ pressure driven instability. The eigenvector of the instability is composed from a sum of several poloidal mode numbers which have different radial distributions. The mode number varies depending on the local- q value so that $m \sim q_{\text{local}}$. For example on JT-60U the mode number near the peak is $m = 4$ and near the plasma edge is $m \sim 6 - 7$. An estimate of the experimental displacement, from the ECE data, is shown for TFTR. The maximum displacement is 5 mm.

As indicated earlier the stability properties are sensitive to various aspects of the plasma profiles. In order to explore this we now turn our attention to the analysis of model equilibria with a q -profile which has a low shear region at a radius $r/a \sim 0.5$. We select a pressure profile which has a very localized gradient, located near the low shear region, see the inset in Fig.5. We determine the stability limits by examining several equilibria which have a fixed q -profile and the same functional form of the pressure profile with increasing β . Rather than report the result in terms of a global measure of β we use the local pressure gradient and determine the maximum stable value, α_{local} , where $\alpha \equiv -\frac{2Rq^2}{B^2} \frac{dp}{dr}$. This value varies with the local q -value, (q_{local}), here q_{local} is measured at the location of the maximum pressure gradient. By scaling the toroidal field we can also determine the effect of varying q_{local} .

The composite stability threshold curve is shown in Fig. 5, which also includes a typical

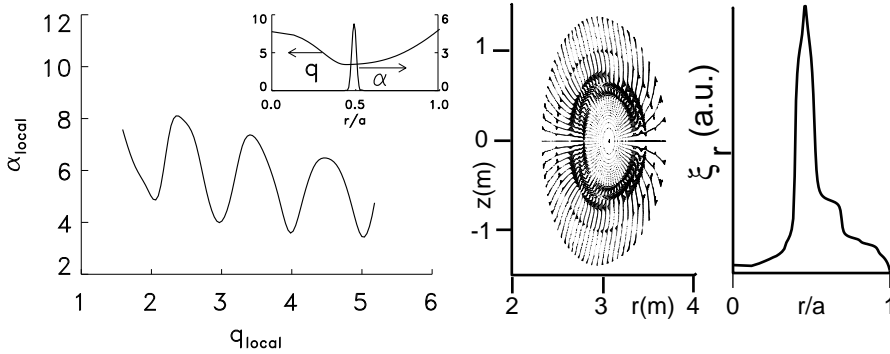


Figure 5: The stability limit of the $n = 1$ mode expressed in terms of the local pressure gradient and its dependence on the local- q value. An example of the model profiles used to determine this curve is shown in the inset. The dependence on q_{local} is determined by scaling the toroidal field. The mode structure of the instability is shown on the right hand side. The dominant poloidal mode number is $m \sim q_{\text{local}}$.

eigenfunction for the localized $n = 1$ instability. Although it is not shown in the figure, we note that the corresponding values of β_N are quite low ranging from 0.2 to 0.6. The extreme localization of the pressure gradient is responsible for reducing the β threshold: when the pressure gradient is distributed over a wider radius, then the stability threshold rises to β_N values between 1 and 2. The other notable feature of this figure is the strong sensitivity to the proximity of integer- q to the minima in the maximum allowable pressure gradient. This feature mimics the more familiar plots of β_N vs q_{min} [11], and indeed gives us a clue to the origin of that variation. The results shown here were obtained in a geometry corresponding to JT-60U. Similar analysis and results are obtained for the circular TFTR like case, the main difference is that the stability thresholds are lower in the circular case.

The model profiles used in producing Fig. 3 are extreme examples in the sense that the pressure gradient is very localized and is located at the point of lowest shear. They were used to illustrate the critical dependence of the stability on the characteristics of the plasma p and q profiles. Usually the experimental profiles have pressure gradients which are more distributed and are not located exactly at the point of lowest shear. To understand this dependence we have examined a large range of profiles which are better representations of the experimental data. Based on this analysis a theoretical model for the observed MHD activity can be constructed.

The main features of the model are as follows; (a) A large pressure gradient in a low shear region drives a localized mode, this implies that if the pressure gradient is shifted away from the low shear region the mode can be stabilized. (b) The position of rational surfaces relative to the peak in the pressure gradient is important. (c) The radial extent of the internal mode depends on the gradients in the p and q profiles, and also depends on the value of q_{min} , the mode width increases as q_{min} decreases. (d) The internally driven mode can couple to the plasma edge, the strength of the coupling depends on q_{edge} , being strongest when q_{edge} has a value slightly less than an integer, *e.g.* 6.8, and also depends on the current density near the plasma edge. (e) The internal mode can couple to energetic particles in the vicinity resulting in a modified growth-rate for the instability. Depending on the precession velocity of the fast particles, the effect may be stabilizing or destabilizing, local radial electric fields can also play a role in determining the role of energetic particles.

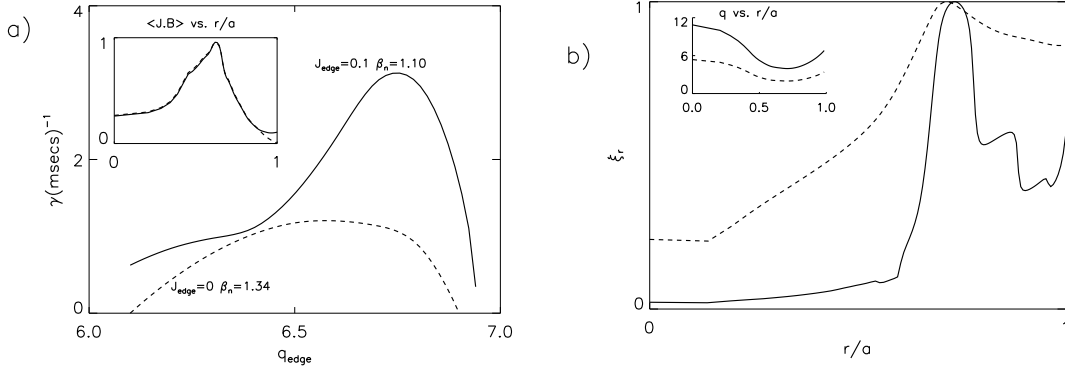


Figure 6: **a.** Dependence of the growth-rate on plasma current density near the edge. Note that when the edge current density is reduced to zero, at $\beta_N = 1.1$ the mode is completely stable. It is destabilized when β is increased to $\beta_N = 1.34$, and the sharp peak of the growth-rate near $q_{\text{edge}} = 6.8$ is eliminated as the coupling to the external kink is reduced. **b.** The radial structure of the instability for $q_{\text{min}} = 4$ and $q_{\text{min}} = 2$, in each case $\beta_N = 1.1$ and the pressure profile shape was held constant. Note that as q_{min} is reduced the width of the mode increases and becomes comparable to the plasma radius.

The first two points of this model have been discussed in the context of Fig. 5, we now address point (c). The effects of the edge current density, q_{edge} and q_{min} are illustrated in Fig. (6a), which shows the effect of modifying J_{edge} and q_{edge} on the growth-rate. In this study the pressure profile is kept constant, $\beta_N = 1.1$, and as before the q -profile is varied by scaling the toroidal field. The inset in Fig. (6a) shows the radial profile of $\langle J \cdot B \rangle$ for the base case (solid curve). Note the finite current density at the plasma edge. A modified profile with zero edge current is also shown as a broken curve. The growth-rate of the ideal $n=1$ instability for the base case shows a sharp onset and rise as q_{edge} is reduced below an integer value. A further reduction of q_{edge} reduces the growth-rate but does not stabilize the mode. We attribute the peak in the growth-rate at $q_{\text{edge}} \sim 6.8$ to a strong coupling to the current driven external kink. Analysis of the modified equilibrium with zero current at the edge shows that it is stable when $\beta_N = 1.1$. However increasing the β so that $\beta_N = 1.34$ destabilizes the internal mode and the resulting growth-rate dependence on q_{edge} is shown as a broken curve in Fig. 5a. We note that the additional peak $q_{\text{edge}} \sim 6.8$ due to coupling to the external kink is absent. The dependence of γ on the q_{edge} however suggests that there is still some residual contribution from the current drive term.

In Fig. 6b we show the effect of lowering q_{min} on the mode structure. The q -profiles are shown in an inset, the profile with $q_{\text{min}} = 4$ is the same one used in Fig. 4 for the JT-60U analysis. The pressure profile is also that of Fig. 4. We now generate a distinct new equilibrium with the same pressure profile shape and a modified q -profile with $q_{\text{min}} = 2$, (broken curve in inset), with $\beta_N = 1.1$. The mode structure of the instabilities in the two equilibria are shown as solid and broken curves in Fig. 5b. The mode structure is composed of a sum of several poloidal mode numbers, the dominant ones are $m = 4$ when $q_{\text{min}} = 4$ and $m = 2$ when $q_{\text{min}} = 2$. This is consistent with the expectation that $m = nq$ plays an important role in determining stability. However the dramatic change in the mode width as q_{min} is reduced suggests that if such an equilibrium were obtained in the experiment, the instability would have a larger effect on the discharge than the brief localized bursts observed when $q_{\text{min}} = 4$.

We now discuss (d), the role of energetic particles. In a different discharge on TFTR, (TFTR:104977), the BLMs were also observed, however stability analysis of this equilibrium shows that the ideal MHD mode is stable. Unlike TFTR:96051 this discharge has strong electric fields, (Fig. 3), at the time of the BLMs. The electric field is determined directly from the MSE data, as well as from a force balance equation using the measured toroidal and poloidal flows[12,13]. In order to account for the electric field we examine the role of the energetic particles. We start from the dispersion relation for the $m = 1$ fishbone,

$$\sqrt{\omega(\omega - \Omega_*)} \sim i\gamma_{\text{MHD}}\left(1 + \frac{\delta W_{\text{k}}}{\gamma_{\text{MHD}}}\right).$$

Here Ω_* represents the ion diamagnetic frequency, γ is the growth-rate of the ideal MHD mode in the single fluid limit, note that $\gamma = \sqrt{(-\omega_{\text{MHD}})^2}$ and δW_{k} represents the contribution of the fast particles interacting with the MHD eigenfunction. The main point to note is that even though this relation was derived specifically for the $m = 1$ mode, the question of stability is determined primarily by the value of $Re(\delta W_{\text{k}})$, while the imaginary part determines the frequency shift. However, it should be noted that unlike the case of the $m = 1$ fishbone, both passing and trapped particles contribute to the kinetic interaction in this case. The expression for this term is

$$Re(\delta W_{\text{k}}) \propto \beta_{\text{hot}} \int \frac{dE dr}{\omega - \omega_{\text{prec}} - \Omega_{E \times B}}.$$

Here β_{hot} represent the number of fast particles, dE is the increment of energy due to the particle's interaction with the MHD mode structure, ω is the mode frequency, ω_{prec} represents the precession frequency in the absence of an electric field and $\Omega_{E \times B}$ represents the modification to the precession frequency due to the radial electric field, E .

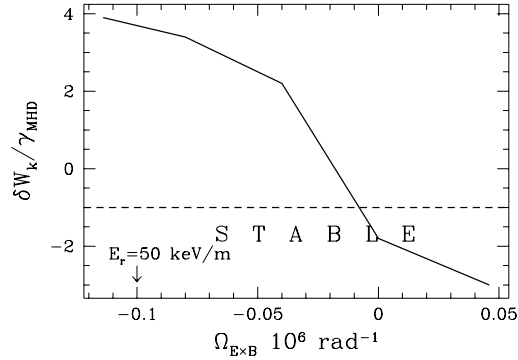


Figure 7: A strong negative electric field can kinetically destabilize an $m > 1$ internal mode.

Using the profiles and mode structure from TFTR:96051 and assuming that $\omega \sim \omega_{\text{prec}}$, (12 kHz), we examine the effect of the electric field. In TFTR $\beta_{\text{hot}} \sim 1\%$ which is about 20% of the total β near the core, consequently we expect that this interaction could be significant. Fig. 7 shows the dependence of $\frac{\delta W_{\text{k}}}{\gamma_{\text{MHD}}}$ on the electric field through the frequency shift in the resonant denominator of the expression for δW_{k} . We see that, as the electric field becomes large and negative, the contribution of the fast particles to the growth-rate of the instability increases. In the figure we have normalized the growth-rate to that of an ideal MHD instability with $\gamma = 12\text{msec.}^{-1}$, the growth-rate observed in the analysis of TFTR:96051. The interpretation of this figure is that when the additional rotation due to the electric field is such that $\frac{\delta W_{\text{k}}}{\gamma_{\text{MHD}}} < -1$ the mode is stabilized. If it is greater than unity, then the kinetic effects are dominant and destabilizing. Figure 7 shows that a radial electric field of about 50 kV/m, corresponding to

$\Omega_{E \times B} = -1 \times 10^6 \text{ rad}^{-1}$ (16 kHz) will cause a strong destabilization of the mode. It is interesting to note that in the first case, where the single fluid ideal MHD model predicts instability, there is no indication of a large electric field from the MSE data, while in the case where the ideal model predicts stability, a strong radial electric field capable of destabilizing the instability is observed. We have also examined the JT-60U case for the role of fast particles, however since $\beta_{\text{hot}} \sim 0.1\%$ we do not find any significant change in the ideal MHD growth-rate.

3 Discussion

The model presented here is based on linear theory and is limited to identifying the conditions for the onset of the instabilities. The nonlinear consequences of these instabilities lie beyond the scope of this report, but based on the mode structure, growth-rate and sensitivity to profile details we offer some general remarks on the possible consequences of these instabilities. The discharges studied here are not in steady state but are continually evolving as the current is continuing to be ramped up, the local transport properties are changing and external heating is applied. It is therefore necessary to consider a range of scenarios to understand the discharge. In the early phases of the discharge, when q_{min} is close to an integer and has a value greater than two, the mode would tend to be more localized. This allows for the possibility of a relaxation and recovery phenomenon, where the local pressure gradient is redistributed by the instability. In the case of JT-60U the large radius for shear reversal also permits a strong coupling to the edge. This suggests that when q_{min} is close to integer and q_{edge} is slightly smaller than an integer then the mode may cause a β collapse as the internal drive couples to the external drive. However if only one of the conditions is met then the instability has less of an effect on the plasma stored energy. In the latter case the main consequence might be to temporarily reduce the local pressure gradient which may permit safe transition through this region until the next rational surface appears at either q_{min} or q_{edge} . However such a conjunction when q_{min} is low, *e.g.* $q_{\text{min}} \sim 2$, would be more devastating as the growth-rate is greatly increased and the mode width becomes comparable to the plasma radius. In TFTR at high q_{min} , the mode does not cause a β collapse because of the smaller ITB radius, however because of the relatively large contribution of the fast particle β , there is a coupling to the mode which results in a fishbone like time evolution. Local radial electric fields are an additional destabilizing feature in this regime.

In summary, we have examined the ideal MHD stability of JT-60U and TFTR and determined that the BLMs observed in these two devices are due to an $n = 1$ ideal MHD mode driven primarily by the local features of the pressure and q -profiles. The proximity of rational surfaces plays an important role in determining the threshold of the instability.

Acknowledgment: This work was supported by the US Department of Energy under contract No. DE-AC02-76-CH03073. JAERI authors were supported by the Japan Science and Technology Ministry. The authors from Princeton Plasma Physics Laboratory wish to extend their gratitude to JAERI for their hospitality and generous sharing of their experimental data as well as their expertise.

References

- [1] Fujita et al., Nucl. Fusion **38** (1998) 207.
- [2] Ishii et al., Plasma Phys. Control. Fusion **40** (1998) 160.
- [3] Manickam et al., Proc. of the **16th**. IAEA Conf. Montreal 453 (1996).
- [4] Chang et al., Phys. Rev. Lett. **77** (1996) 3553.
- [5] Fredrickson et al., Phys. of Plasma **4** (1997) 1589.
- [6] Ishida et al., Phys. Rev. Lett. **79** (1997) 3917.
- [7] Takeji et al. Phys. Plasmas **4** (1997) 4283.

- [8] Shirai et al., J. Phys. Soc. Japan **64** (1995) 4209.
- [9] Budny et al., Nucl. Fusion **32**, (1995) 1497.
- [10] Grimm et al, Meth. of Comp. Physics **16** (1976) 257.
- [11] Phillips et al., Phys. Plasmas **3** (1996) 1673.
- [12] Levinton et al., Phy. Rev. Lett. **80**, (1998) 4887.
- [13] Bell et al., Phy. Rev. Lett. **81**, (1998) 1429.